Pharm Res (2012) 29:2512–2521
DOI 10.1007/s11095-012-0781-x

RESEARCH PAPER

Anti-Neuropilin-1 (MNRP1685A): Unexpected Pharmacokinetic Differences Across Species, from Preclinical Models to Humans

Yan Xin • Shuang Bai • Lisa A. Damico-Beyer • Denise Jin • Wei-Ching Liang • Yan Wu • Frank-Peter Theil • Amita Joshi • Yanmei Lu • John Lowe • Mauricio Maia • Rainer K. Brachmann • Hong Xiang

Received: 21 December 2011 / Accepted: 14 May 2012 / Published online: 16 June 2012

ABSTRACT

Purpose To compare the pharmacokinetics (PK) of MNRP1685A, a human monoclonal antibody (mAb) against neuropilin-1 (NRP1), in mice, rats, monkeys, and cancer patients from a Phase I study to model with parallel linear and nonlinear clearances.

Methods Binding characteristics of MNRP1685A in different species were evaluated using surface plasmon resonance technology. PK profiles of MNRP1685A after single and/or multiple doses in different species were analyzed using population analysis. PK parameters were compared across species.

Results MNRP1685A binds to NRP1 in all four species tested. Consistent with the wide expression of NRP1, MNRP1685A demonstrated pronounced non-linear PK over a wide dose range. PK profiles are best described by a two-compartment model with parallel linear and nonlinear clearances. Model-derived PK parameters suggest similar *in-vivo* target expression levels and binding affinity to target across all species tested. However, compared to typical human/humanized mAbs, non-specific clearance of MNRP1685A was faster in mice, rats, and humans (60.3, 19.4, and 8.5 ml/day/kg), but not in monkeys (3.22 ml/day/kg).

Conclusions Monkey PK properly predicted the target-mediated clearance of MNRP1685A but underestimated its non-specific clearance in humans. This unique PK property warrants further investigation of underlying mechanisms.

KEY WORDS angiogenesis · MNRP1685A · neuropilin-1 · nonlinear PK

Electronic supplementary material The online version of this article (doi:10.1007/s11095-012-0781-x) contains supplementary material, which is available to authorized users.

Y. Xin • S. Bai • D. Jin • F.-P. Theil • A. Joshi • H. Xiang
Department of Pharmacokinetic and Pharmacodynamic Sciences
Genentech, Inc.
1 DNA Way
South San Francisco, California, USA

L. A. Damico-Beyer
Portfolio Management and Operations, Genentech, Inc.
1 DNA Way
South San Francisco, California, USA

W.-C. Liang • Y. Wu
Department of Antibody Engineering, Genentech, Inc.
1 DNA Way
South San Francisco, California, USA

Y. Lu
Department of Biochemical and Cellular Pharmacology
Genentech, Inc.
1 DNA Way
South San Francisco, California, USA

J. Lowe • M. Maia
Department of Bioanalytical Sciences, Genentech, Inc.
1 DNA Way
South San Francisco, California, USA

R. K. Brachmann
Oncology Exploratory Clinical Development, Genentech, Inc.
1 DNA Way
South San Francisco, California, USA

H. Xiang (✉)
Department of Pharmacokinetic and Pharmacodynamic Sciences
Genentech, Inc.
1 DNA Way, MS 46-3A
South San Francisco, California 94080, USA
e-mail: hxc@gene.com

ABBREVIATIONS

ATA	anti-therapeutic antibody
CHO cells	Chinese hamster ovary cells
CL	non-specific clearance
CL_d	distribution clearance
CV	coefficient of variation
ELISA	enzyme-linked immunosorbent assay
FC	flow cell
FcRn	neonatal Fc receptor
HRP	horseradish peroxidase
IV	intravenous
K_D	equilibrium dissociation constant
kg	kilogram
K_m	drug concentration at 50 % V_{max}
k_{off}	off-rate
k_{on}	on-rate
LLOQ	lower limit of quantitation
mAbs	monoclonal antibodies
mg	milligram
min	minute
ml	milliliter
mM	millimolar
ng	nanogram
nM	nanomolar
NRP1	neuropilin-1
PBS	phosphate-buffered saline
PK	pharmacokinetics
q3w	every three weeks
RSE	relative standard error of estimation
RU	response unit
SD	standard deviation
V_1	apparent volume of central compartment
V_2	peripheral compartment distribution volume
VEGF	vascular endothelial growth factor
V_{max}	maximum drug elimination by nonlinear (or specific) clearance
μg	microgram
μl	microliter
σ_{prop}	proportional residual error
ω_{CL}	inter-subject variability on CL
ω_{Km}	inter-subject variability on K_m
ω_{V1}	inter-subject variability on V_1
ω_{Vmax}	inter-subject variability on V_{max}

INTRODUCTION

There has been a rapid increase in our understanding of the *in vivo* disposition of therapeutic mAbs, partially due to the growing interest in developing mAb drugs over the past two decades. It is generally believed that the PK of therapeutic mAbs is determined by target-mediated (*via* specific antibody-ligand binding) and target-independent (*i.e.*, non-specific Fc-receptor mediated elimination) mechanisms (1–3). The rate of elimination of mAbs by target-mediated clearance is specific for each antibody, and it is dependent on the nature of the specific target (*e.g.* expression level and turnover rate), as well as the binding affinity of the mAb to the target. The rate of elimination of mAbs by target-independent clearance is likely dominated by their binding affinity to the FcRn in a pH-dependent fashion. However, several other factors are important in determining the disposition of mAbs, and these include immunogenicity, the degree and the nature of glycosylation, the ability to bind to Fcγ receptors, and the susceptibility to proteolysis (2,4,5). Despite differences in their pharmacological targets and patient populations, the target-independent or non-specific clearance of therapeutic mAbs currently in clinical use are strikingly similar (1). In addition, for mAbs with typical PK properties, accumulated knowledge suggests that PK data from cynomolgus monkeys alone can be successfully scaled to accurately project human PK profiles within the linear range, using simplified allometry and Dedrick plots with fixed exponents (6,7).

However, there have been a few reports of mAbs that have shown unexpectedly fast clearance, with known or unknown underlying mechanisms. For example, PK of an anti-amyloid beta antibody demonstrated accelerated clearance in cynomolgus monkeys but not in mice, likely due to off-target binding to cynomolgus monkey fibrinogen (8). A humanized antibody against fibroblast growth factor receptor 4 showed fast clearance in mice due to off-target binding to mouse complement component 3 (9). Small differences in CDR3 sequence of an antibody against interleukin 21 led to rapid clearance in mice, rats, and cynomolgus monkeys for unknown reasons (10). Here we report another interesting case of a therapeutic mAb with unexpected PK profiles across species.

The antibody target, NRP1, is a multifunctional receptor widely expressed on endothelial cells and tumor cells (11) that contributes to the development of the nervous and vascular systems. NRP1 was first described as a receptor that binds semaphorin 3A (Sema 3a), acting with the plexins to regulate neuronal guidance (12). It was later shown that NRP1 also binds VEGF to mediate vascular development (13,14). NRP1 mRNA expression levels are relatively high in heart and placenta; more moderate in lung, liver, skeletal muscle, kidney, and pancreas; and relatively low in adult brain (11,14,15). Expressed in endothelial cells (11,14,15), NRP1 is a 130–140 kDa transmembrane protein containing a large extracellular domain (ECD), a single transmembrane domain, and a short cytoplasmic domain (13). The extracelluar domain has three parts: a1a2 as Sema 3a ligand-binding domain; b1b2 as VEGF binding domain, and C (MAM) domain involved in NRP1 dimerization (12,16–18).

There are four naturally occurring, alternatively spliced human soluble NRP1 (sNRP1) (19–21). sNRP1 proteins of 64 kDa in mouse, 75 kDa in rat, 90 kDa in monkey, and 90 and 75 kDa in human serum have been identified. In addition, the circulating NRP1 ECD with a molecular weight of 120 kDa might be present in all these species (22).

MNRP1685A is a phage-derived human mAb that specifically binds to the b1b2 domain of NRP1 and selectively blocks VEGF binding to NRP1. It does not affect binding of semaphorins to NRP1, and therefore it is not expected to interfere with neuronal guidance (23). Several studies have shown a role for NRP1 in tumor biology and have indicated that it participates in the regulation of vascular and/or tumor cell functions (11). By inhibiting the binding of VEGF to NRP1, MNRP1685A has been shown to reduce $VEGF_{165}$-dependent endothelial cell migration and vessel sprouting *in vitro*; to decrease neovascularization and vascular remodeling *in vivo*, and to slow tumor growth in several tumor models, both as a single agent and in combination with anti-VEGF (23–25). The potential of MNRP1685A to improve anti-angiogenic cancer therapy led to the testing of this molecule in Phase I clinical trials, both as a single agent and in combination with bevacizumab, with or without paclitaxel.

MNRP1685A binds to mouse, rat, cynomolgus monkey, and human NRP1 with similar affinity. Thus, its PK properties were evaluated in those three relevant preclinical species to understand the impact of target expression on PK, to predict its PK properties in humans, and to ultimately guide first-in-human study design.

MATERIALS AND METHODS

Dosing Solutions

MNRP1685A was manufactured by Genentech Inc. (South San Francisco, CA) using CHO cells. MNRP1685A stock solutions were prepared in PBS for mouse studies, or in vehicle (20 mM histidine acetate, 240 mM trehalose, 0.02 % polysorbate 20, pH 5.5) for all other studies, and stored at 2–8°C. MNRP1685A was diluted in PBS (for mouse studies), vehicles (for rat and monkey studies), or sterile normal saline (for human study) to desired nominal concentrations for each dosing level.

NRP1 from Different Species

Human, mouse, and cynomolgus monkey NRP1 constructs (1-641aa) were cloned into a mammalian expression vector, expressed in CHO cells, and purified as secreted recombinant protein containing His-tagged or Fc-fusion protein. Recombinant rat NRP1/Fc chimera protein was purchased as lyophilized powder (Catalog 566-N1; R & D Systems; Minneapolis, MN) and resuspended in PBS at 200 μg/ml. These materials were stored at 2–8°C before use.

Surface Plasmon Resonance (BIAcore Technology) Assay

Human NRP1 was coupled onto three separate FCs, FC2, FC3, and FC4, of a BIAcore CM5 sensor chip (BIAcore, Inc., Piscataway, NJ) to achieve RU of approximately 350. Immobilization was achieved by random coupling through amino groups using a protocol provided by the manufacturer (BIAcore, Inc.). Sensorgrams were recorded for binding of MNRP1685A to these surfaces after injection of a series of MNRP1685A solutions ranging in concentration from 0.2 nM to 50 nM, in 2-fold increments, at a flow rate of 30 μl/min at 25°C. Glycine-HCl (10 mM, pH 1.7) was used to regenerate the sensor chip between injections. The signal from the reference FC1 was subtracted from the signals measured in FC2, FC3, and FC4. Kinetic constants were calculated by nonlinear regression fitting of the data according to a 1:1 Langmuir binding model using BIAcore evaluation software (version 3.2) supplied by the manufacturer. The same approach was used for determining binding kinetics and affinity constants of MNRP1685A to mouse, rat, and cynomolgus monkey NRP1.

Mouse PK Studies

The PK study in athymic nude nu/nu mice was approved by the Institutional Animal Care and Use Committee (IACUC) and conducted at Genentech, Inc. As summarized in Table I, PK data from 5 single-dose and 4 multiple-dose studies were pooled together to cover a wide range of dose levels (from 0.5 to 150 mg/kg) at various time points post dose, with 1–3 blood draws per mouse. All studies were conducted in female athymic nude nu/nu mice, with or without tumor, and used IV administration of MNRP1685A. Group average serum concentrations at the same time point (n=3 mice/time point) were used for PK analysis.

Rat PK Study

The PK study in Sprague–Dawley rats was approved by the IACUC and conducted at Genentech, Inc. Three female Sprague-Dawley rats (Charles River Laboratories, Hollister, CA) were assigned to each of three dosing groups at 2, 10, or 50 mg/kg. Each group received a single IV bolus dose of MNRP1685A in the tail vein. Blood samples were collected

Table I Summary of Mouse PK Studies

Study	Dose Regimen	Sampling Scheme	Tumor-bearing
1	0.65, 10, 100 mg/kg; single dose	15 min to 28 days post dose	No
2	10, 100 mg/kg; single dose	15 min to 21 days post dose	No
3	10, 40, 120 mg/kg; single dose	4 hr to 14 days post dose	Yes
4	40, 80 mg/kg; 3 weekly doses	15 min post dose, 30 min predose	Yes
5	5, 10, 20, 40 mg/kg; 3 weekly doses	4 days post last dose	Yes
6	2.5, 20, 80 mg/kg; single dose	4 hr to 7 days post dose	Yes
7	A: 28, 32, 55 mg/kg, day 0, 5, 10; B: 48 mg/kg, day 0, 5; C: 75, 90, 150 mg/kg, single dose	A & B: 1 or 2 days post dose C: 1, 7, 12 days post dose	Yes
8	5, 10, 20, 40 mg/kg, 9 weekly doses	1, 4, or 5 days post 1st, 2nd, or last dose	Yes

at pre-dose and at various time points post dose, ranging from 15 min to 28 days.

Monkey PK Studies

The single-dose and multiple-dose PK studies in cynomolgus monkeys were approved by the IACUC and conducted at SNBL USA, Ltd (Everett. WA) and at Charles River Laboratories (Sparks, NV), respectively.

In the single-dose study, two male and two female monkeys were assigned to each of the four dosing groups (0.5, 3, 15, or 50 mg/kg). Each animal received a single IV bolus dose of MNRP1685A. Blood samples were collected at pre-dose and at various time points post dose, ranging from 10 min to 56 days. ATA samples were collected at pre-dose and at various time points up to 56 days post dose.

In the multiple-dose study, six male and six female monkeys were assigned to each of three dosing groups (10, 30, and 100 mg/kg). Each animal received nine weekly doses of MNRP1685A by IV bolus administration. Blood samples were collected at pre-dose and at various time points post the 1st, 3rd, 5th, 7th, and 9th (last) doses. ATA samples were collected prior to the 1st, 5th, and last doses; as well as 28 and 84 days after the last dose.

Human PK Study

Institutional review boards at each study site approved the protocol, and all subjects provided written informed consent. Human PK data were collected from a Phase Ia study in 30 patients with advanced solid malignancies, who received IV infusion of MNRP1685A as a single agent q3w, at doses of 2, 5, 10, 15, 20, 30, and 40 mg/kg (26). Several serum PK samples were collected during dosing cycle 1, in addition to multiple peak and trough samples from later dosing cycles. Multiple pre-dose ATA samples were collected at different cycles.

Serum Assays

MNRP1685A concentrations in mouse and rat samples were determined using an ELISA, in which recombinant murine NRP1 (His-tagged) was used to coat ELISA plates and capture MNRP1685A. A HRP-labeled goat $F(ab')_2$ anti-human IgG Fc conjugate (Jackson ImmunoResearch Laboratories, Inc.; West Grove, PA) was used for detection of captured drug. The assay's LLOQ in mouse and rat serum was 0.4 ng/ml. The concentration of MNRP1685A in monkey and human serum samples was also determined using an ELISA in which recombinant-human NRP1 (His-tagged) was used as the capture reagent. In the monkey assay, sheep anti-human IgG (monkey adsorbed) HRP conjugate (The Binding Site, Inc.; San Diego, CA) was used as the detection reagent. The assay's LLOQ was 27.4 ng/ml. In the validated human assay, MNRP1685A was detected using a mAb specific to the Genentech IgG framework (mAb 10C4), labeled with biotin. This step was followed by addition of Avidin D-HRP conjugate (Vector Laboratories, Inc.; Burlingame, CA). The assay's LLOQ was 75 ng/ml. The inter- and intra-day CV% values for all the assays were within an acceptable level of 20%.

The presence of ATA in cynomolgus monkey serum and human serum was detected using a bridging ELISA. The assay used MNRP1685A conjugated to biotin and MNRP1685A conjugated to digoxigenin to capture antibodies directed against MNRP1685A, with streptavidin coated on ELISA plates as the capture reagent and mouse anti-Digoxin HRP (Jackson ImmunoResearch Laboratories, Inc.; West Grove, PA) as the detection reagent.

Population PK Analysis

MNRP1685A serum concentration-time profiles in all species were modeled using a two-compartment model comprised of parallel linear and non-linear clearance pathways.

The linear clearance refers to CL through Fc-mediated elimination. The nonlinear clearance or target-mediated clearance is driven by the pharmacological target and was approximated by a Michaelis-Menten equation (3,27), where V_{max} represents the maximum drug elimination by nonlinear (or specific) clearance and K_m indicates the drug concentration at 50 % V_{max}. The differential equations are shown below:

$$\frac{dA_1}{dt} = -[(\frac{V_{max}}{K_m + \frac{A_1}{V_1}})/V_1 + \frac{CL}{V_1} + \frac{CL_d}{V_1}] \times A_1 + \frac{CL_d}{V_2} \times A_2$$

$$\frac{dA_2}{dt} = \frac{CL_d}{V_1} \times A_1 - \frac{CL_d}{V_2} \times A_2$$

Inter-individual variability on CL, V_1, V_{max} or K_m was evaluated when appropriate. A proportional error model was used to describe the residual variability. Concentrations below LLOQ were censored for model fitting. The model-based population PK analysis was performed in NONMEM version VI (ICON Development Solutions, Ellicott City, MD).

Comparison of Observed and Predicted Human PK

In support of the Phase Ia study, MNRP1685A PK parameters were predicted based on cynomolgus monkey data (including data from both single dose and multiple dose studies) using the species time-invariant method (28) as monkeys have been shown to be a reliable species for prediction of human PK of typical mAbs (6,7). A scaling exponent of 0.85 for clearance and of 1 for central compartment volume was used (6). For comparison with human PK profiles observed in the Phase Ia study, 1000 rounds of Monte-Carlo simulations were performed using the projected human PK parameters at the Phase Ia dosing regimen. The 90 % prediction intervals of the MNRP1685A concentration at each time point were calculated with the simulated data and then overlaid with observed human data by dose levels.

RESULTS

Affinity of MNRP1685A to NRP1 Across Species

To better understand the disposition of MNRP1685A across species, the binding affinity of MNRP1685A to NRP1 from different species was assessed by surface plasmon resonance analysis (BIAcore technology). The kinetic constant, K_{on}, K_{off}, K_D of MNRP1685A for human, cynomolgus monkey, rat and mouse NRP1 are summarized in Table II. MNRP1685A binds to NRP1 from human, monkey and mouse with similar affinity, with K_D values ranging between 0.03 and 0.04 nM. However, this is approximately 5- to 7-fold higher than MNRP1685A's estimated K_D for rat NRP1.

MNPR1685A Serum Concentration-Time Profiles in Nonclinical Species

MNRP1685A displayed typical nonlinear kinetics following single IV administration in mice, rats, and cynomolgus monkeys, with non-paralleled concentration-time profiles across all tested dose levels (Fig. 1). In all three species, MNRP1685A cleared rapidly from the system at low concentrations (below ~10 μg/ml), suggesting a dominant role played by target-mediated clearance below this concentration. Therefore, further analysis using a semi-mechanism-based PK model was performed to dissect the role of target-mediated clearance and non-specific clearance mechanisms in the PK profile of MNRP1685A. A population modeling approach was applied to account for inter-individual variability.

MNRP1685A Population PK Parameters in Nonclinical Species

A two-compartment model with parallel linear and non-linear clearance was used to analyze the PK data from each of the three species. Figure 1 and goodness-of-fit plots (Supplementary Material) show good model-fitting of the data. All population PK parameters were estimated with reasonable precision, with acceptable small relative standard error of estimation (%RSE) on key PK parameters (Table III).

For nonlinear (or target-mediated) clearance, the model-derived parameter V_{max}, which reflects target expression, was similar with estimated values of 759 (±168), 824 (±23.9), and 591 (± 21.6) μg/day/kg in mice, rats, and monkeys, respectively. The model-derived K_m value, which

Table II Binding Kinetic and Affinity Analysis of MNRP1685A Across Species

Analytes	Human NRP1	Mouse NRP1	Rat NRP1	Cynomolgus monkey NRP1
k_{on} (10^5 $M^{-1}s^{-1}$)	42 ± 2	91 ± 10	75 ± 15	53 ± 3
k_{off} (10^{-4} s^{-1})	1.8 ± 0.2	2.7 ± 0.7	15.7 ± 3.8	1.7 ± 0.4
K_D (nM)	0.04 ± 0.01	0.03 ± 0.01	0.21 ± 0.03	0.03 ± 0.01

K_D = equilibrium dissociation constant, calculated as the ratio k_{off}/k_{on}; k_{off} = off-rate; k_{on} = on-rate. Note: data were fitted with a 1:1 Langmuir binding model and averaged from three independent studies

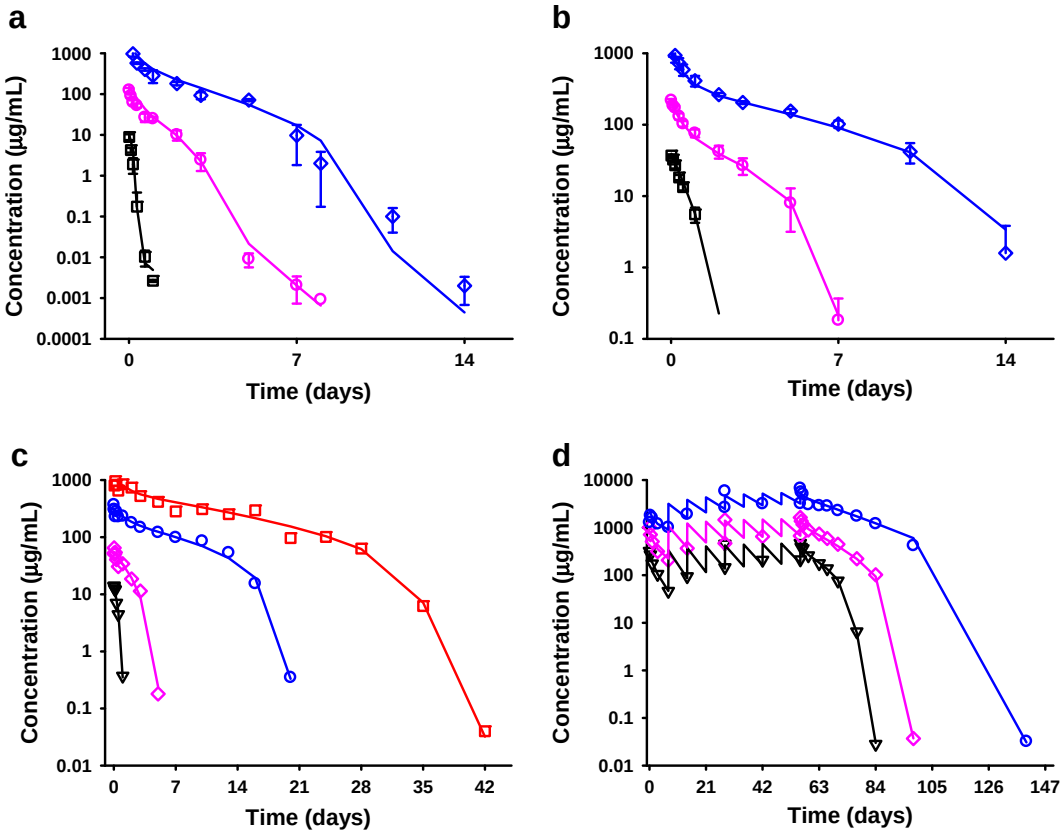

Fig. 1 Observed (open symbols) and model predicted (lines) MNRP1685A concentration-time profiles in mice, rats, and cynomolgus monkeys. (**a**) represents mice receiving a single dose of MNRP1685A at 0.65, 10, and 100 mg/kg (black, pink, and blue, respectively). (**b**) represents rats receiving a single dose of MNRP1685A at 2, 10, and 50 mg/kg (black, pink, and blue, respectively). (**c**) represents cynomolgus monkeys receiving a single dose of MNRP1685A at 0.5, 3, 15, and 50 mg/kg (black, green, blue, and red, respectively). (**d**) represents monkeys receiving multiple doses of MNRP1685A at 10, 30, and 100 mg/kg (black, pink, and blue, respectively).

reflects the *in-vivo* target-molecule binding affinity, was 0.190 µg/ml (~1.3 nM), 0.505 µg/ml (~3.5 nM), and 1.09 µg/ml (~7.5 nM) for mice, rats, and monkeys, respectively.

Interestingly, the model-derived linear (non-specific) clearance was higher than that of typical human IgG1 mAbs (6) in mice (60.3±4.22 ml/day/kg) and rats (19.4±4.56 ml/day/kg), but not in monkeys (3.22±0.17 ml/day/kg). Similarly, CL_d, V_1 and V_2 were consistent with typical IgG1 mAbs in monkeys but high in mice and rats (Table III).

MNRP1685A PK in Humans

MNRP1685A PK was evaluated in cancer patients at doses of 2–40 mg/kg q3w with IV infusion. As expected from the target biology, MNRP1685A demonstrated strong nonlinear PK in humans at lower doses. At doses above 10 mg/kg, the mean serum concentration-time profiles by dose levels were approximately parallel to each other within q3w dosing interval, suggesting that the saturation of the target-mediated clearance was approached (Fig. 2a). However, the observed human concentrations were outside of the 90 % prediction interval projected based on cynomolgus monkey data (Fig. 2b).

As in preclinical species, the concentration-time profiles in human were adequately described by the same two-compartment model with parallel linear and nonlinear clearance [Table III and goodness-of-fit plots (Supplementary Material)]. The estimated target-mediated clearance parameters V_{max} and K_m in humans were ~429 µg/day/kg and 1.35 µg/ml, respectively, for a typical patient (with body weight of 75.5 kg). These values were close to the predicted values of 372 µg/day/kg (V_{max}) and 1.05 µg/ml (K_m) based on cynomolgus monkey PK data. Surprisingly, the non-specific clearance in humans appeared to be over 4-fold faster than the predicted (8.53 *versus* 2.0 ml/day/kg). This was also faster than the non-specific clearance reported for other IgG1 mAbs such as bevacizumab against VEGF (2.8 ml/day/kg) (29), trastuzumab against Her2 (3.2 ml/day/kg) (30), or pertuzumab against Her2 (3.1 ml/day/kg) (31) at their respective therapeutic doses. The distribution parameters V_1, V_2 and CL_d were also higher than cynomolgus monkey-based predictions.

Table III Population PK Parameter Estimates for MNRP1685A

Parameters (unit)	Point Estimate (%RSE)[a]				
	Mouse	Rat	Cyno	Human_predicted [b]	Human_observed [c]
V_{max} (μg/day/kg)	759 (22.1)	824 (2.90)	591 (3.65)	372 (3.41)	429 (15.9)
K_m (μg/ml)	0.190 (23.6)	0.505 (131)	1.09 (4.87)	1.05 (22.4)	1.35 (45.2)
CL (ml/day/kg)	60.3 (7.00)	19.4 (23.5)	3.22 (5.28)	2.00 (4.86)	8.53 (17.2)
V_1 (ml/kg)	62.1 (8.58)	50.1 (29.9)	37.8 (3.52)	37.9 (2.93)	51.0 (9.07)
CL_d (ml/day/kg)	62.6 (11.3)	56.1 (57.8)	12.4 (3.37)	7.72 (9.39)	19.6 (14.3)
V_2 (ml/kg)	54.5 (14.0)	61.7 (42.3)	27.4 (2.47)	27.4 (3.54)	79.1 (11.9)
ω_{Vmax}, %	34.1 (56.5)	NA	11.0 (62.5)	9.74 (42.2)	NA
ω_{Km}, %	NA	NA	NA	NA	131 (54.2)
ω_{CL}, %	18.6 (38.7)	NA	27.9 (24.7)	26.4 (27.0)	35.8 (58.1)
ω_{V1}, %	NA	NA	17.2 (33.8)	17.1 (23.4)	23.7 (68.8)
σ_{prop}, %	29.0 (21.8)	28.7 (30.9)	12.7 (5.77)	13.3 (14.5)	24.3 (5.06)

a. %RSE = percent of relative standard error of estimation

b. Predicted based on cynomolgus monkey PK data

c. Adapted from(1), PK parameters normalized by median body weight (75.5 kg) of patients

Cyno = cynomolgus monkeys; CL = linear (or non-specific) clearance; V_{max} = maximum drug elimination by nonlinear (or specific) clearance; CL_d = distribution clearance; V_1 = apparent volume of central compartment; V_2 = peripheral compartment distribution volume; K_m = drug concentration at 50 % V_{max} (μg/mL); ω_{Vmax} = inter-subject variability on Vmax; ω_{Km} = inter-subject variability on K_m; ω_{CL} = inter-subject variability on CL; ω_{V1} = inter-subject variability on V1; σ_{prop} = proportional residual error; NA = not available

The Impact of ATAs on PK

The target-mediated clearance could be confounded by clearance mediated by ATA (2). In monkeys, the ATA incidence was 69 % (11/16) and 19 % (7/36) after single- and multiple-dose administration, respectively. The timing of ATA onset after MNRP1685A administration ranged from 21 to 56 days (single-dose study) and 28 to 140 days (multiple-dose study). In the single-dose study, ATA-positive animals had PK profiles similar to ATA-negative animals, with comparable estimated non-specific clearance (data not shown). In the multiple-dose study, since lower PK exposure correlated with the presence of ATA, drug concentration measurements outside of 5 standard deviations from the mean in positive ATA samples were excluded from model fitting (3.7 % of total data records). Therefore,

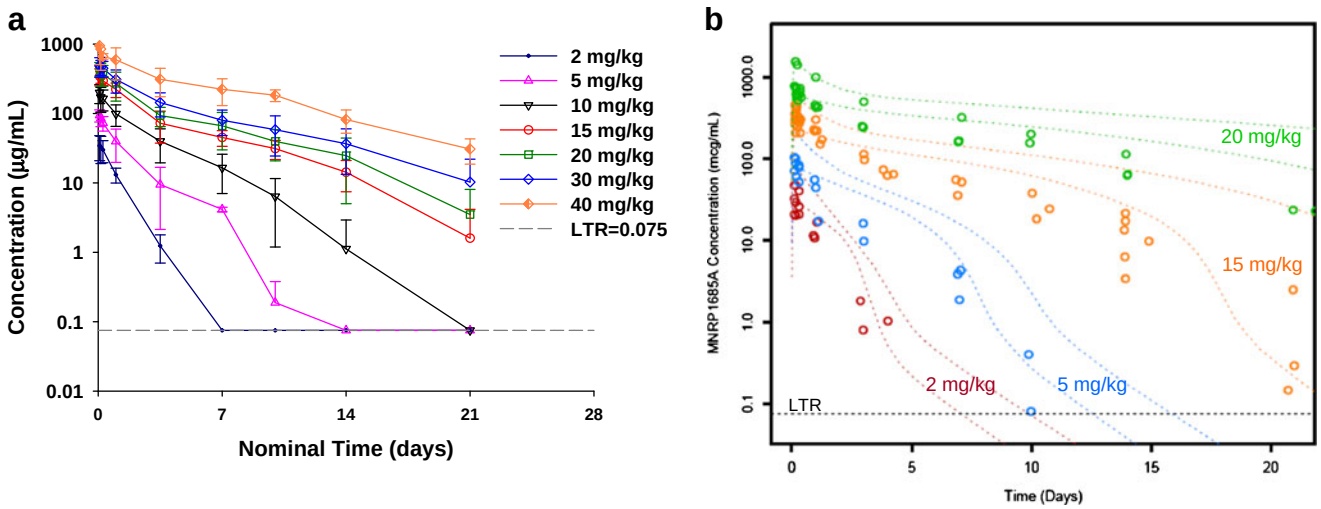

Fig. 2 Observed mean concentration-time profiles of MNRP1685A in human and comparison with cyno-based prediction. (**a**) corresponds to the observed human mean concentration-time profiles (Cycle 1) by dose (n=3 for 2, 5, 10, 30, and 40 mg/kg; n=6 for 10 and 15 mg/kg). (**b**) corresponds to the observed human concentrations (open circles) *versus* 90% prediction interval (dotted lines) based on cynomolgus monkey data.

the observed fast clearance in cynomolgus monkeys at serum concentrations ≤10 μg/ml appears to be truly *via* target-mediated clearance.

The immunogenicity response was not expected in the immune-deficient athymic nude mice. Although ATA was not tested in rats, the PK profile did not demonstrate the typical ATA-mediated clearance commonly observed in rats. In humans, none of the patients tested positive for ATA, suggesting that target-mediated clearance was the main driver for the observed fast clearance at lower doses.

DISCUSSION

The current study evaluated MNRP1685A PK in mice, rats, cynomolgus monkeys, and humans. Consistent with the wide expression of target NRP1, MNRP1685A demonstrated strong target-mediated clearance in all species tested, resulting in pronounced non-linear PK over a wide range of doses. The concentration-time profiles are best described by a two-compartment model with parallel linear and nonlinear clearances.

The nonlinear clearance is driven by the amount of pharmacological target in the body and often refers to target-mediated clearance. The main characteristic of target-mediated clearance is that the dose-normalized concentration-time profiles are not superimposable, as illustrated in Figs. 1 and 2a for MNRP1685A. This pronounced nonlinear PK property of MNRP1865A is consistent with saturable binding sites in lungs, liver, and kidneys, as observed in mouse tissue distribution studies (32).

In the population PK analysis, the model-derived PK parameter V_{max} suggests that the *in-vivo* target expression levels are similar in mice, rats, cynomolgus monkeys, and humans. This is supported by a tissue cross-reactivity study with MNRP1685A, in which the specific staining of NRP1 was shown to be similar in cynomolgus monkey and human tissues (data not shown). In another study, the baseline circulating NRP1 was found to be comparable in cynomolgus monkeys and humans (22). However, rat is qualitatively and quantitatively different from the other species, since the specific staining of MNRP1685A to NRP1 in rat is lighter than that in cynomolgus monkeys and humans (data not shown) and the baseline circulating NRP1 is lower in rat than in the other three species (22). Of note, the model-derived K_m value is much higher than *in vitro* K_D for all species. This discrepancy may be explained, based on recent publication, that *in vivo* K_m is the sum of K_D and the ratio of the internalization rate constant (k_{int}) and k_{on} (27).

It is worth noting that for molecules with nonlinear PK, target-mediated clearance always contributes to the total clearance, even at high concentrations. However, the extent of target-mediated clearance depends on the abundance of the target (reflected on V_{max} value). As shown in Fig. 3, MNRP1685A, panitumumab (a fully human monoclonal IgG2 which targets a widely expressed epidermal growth factor receptor (33)), and sibrotuzumab (a humanized monoclonal mAb which targets the less widely distributed fibroblast activation protein (34)) have different nonlinear PK profiles resulting from different target expression levels. NRP1 is expressed at high levels in a wide variety of tissues (11), thus even at 134 μg/ml of MNRP1685A (~99 % saturation of target-mediated clearance), the linear clearance only accounts for 67 % of total clearance of MNRP1685A in humans. Similarly, panitumumab showed only 50 % contribution of non-specific clearance at 99 % saturation of target-mediated clearance (43 μg/ml). In contrast, for sibrotuzumab, the target-mediated clearance is less significant, thus when target binding is 99 % saturated, the linear clearance plays a dominant role (94 % of total clearance) for this mAb.

Due to the uncertainty and inherent biological variability associated with target characteristics, it is commonly acknowledged that scaling of target-mediated clearance of mAbs is difficult (6). However, this was not the case for

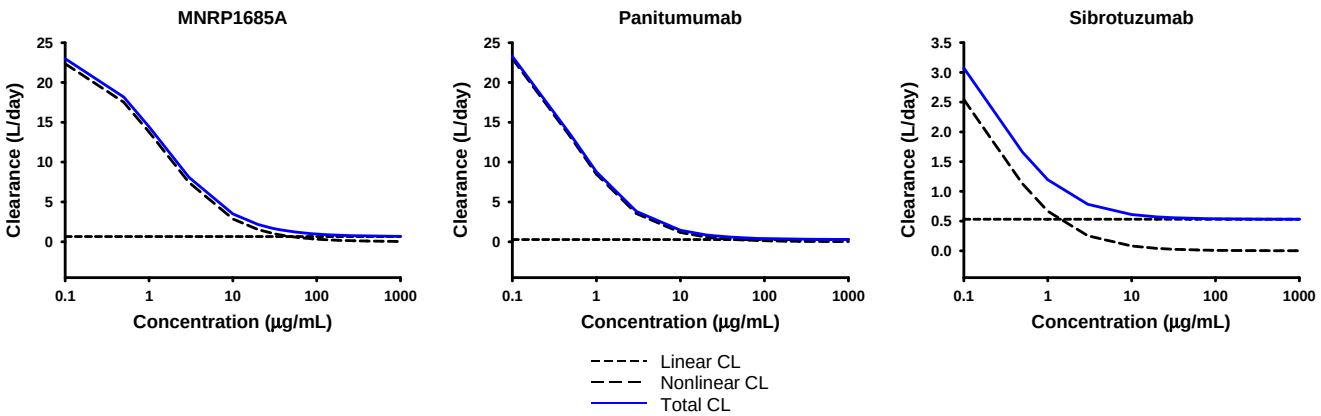

Fig. 3 Examples of dependence of clearance on concentration in humans. The blue solid lines represent total CL. The short dashed lines represent nonlinear CL. The long dashed lines represent non-specific CL. Nonlinear CL=V_{max}/(K_m + Concentration). Total CL=Linear CL + Nonlinear CL.

MNRP1865A. Although NRP1 expression was reported to be increased by 2- to 3-fold in high-grade dysplasia, invasive cancers, and metastases of the human gastrointestinal tract (35), the difference of antigen load amongst Phase I patients was mostly due to inter-subject variability (Table III) and might not be significant enough to affect predictability of target-medicated clearance of MNRP1685A in humans based on cynomolgus monkey data.

Surprisingly, in the present study, MNRP1685A showed faster non-specific clearance in mice, rats, and humans, although it has the same human IgG1κ backbone and biochemical characteristics (such as glycosylation, percentage of aggregation, *etc.*) as trastuzumab, bevacizumab, and pertuzumab, and was expected to show similar non-specific clearance to those mAbs. We also observed that monkey PK data properly predicted MNRP1685A's target-mediated clearance, but underestimated its non-specific clearance in humans, with a 4-fold difference between the observed (8.53 mL/day/kg) and the predicted (2.0 ml/day/kg) values. To our knowledge, this is the first reported case in which cynomolgus monkey is found to be a poor predictive species of human PK for a human IgG1 mAb with binding to target across species.

Although the causative mechanism for this observation is not clear, there have been studies aimed at better understanding the reasons for the unexpected cross-species difference in non-specific clearance of MNRP1685A. One interesting finding has been that MNRP1685A has a slower elution time on size-exclusion chromatography than mAbs with typical nonspecific clearance, suggesting unique characteristics of MNRP1685A in its conformational structure, which may contribute to off-target binding in mice, rats, and humans (data not shown). In addition, MNRP1685A was found to induce platelet reduction in patients but not in monkeys (36). Further *in vitro* studies demonstrated CD32 (FcγRIIa)-dependent and -independent MNRP1685A binding to human platelets (36). Whether there is differential platelet binding in humans and monkeys and whether it can account for the faster non-specific clearance observed in patients is still under investigation. Based on currently available data, we speculate that the unexpected PK profile of MNRP1685A is likely due to unsaturable off-target binding.

Our experience with MNRP1685A provides significant insights into selection considerations for future drug candidates. If the non-specific clearance in any of the preclinical species is different from typical IgG1 mAbs, it may indicate a potential PK risk for that molecule. Two recent studies have described interesting findings related to off-target binding of mAbs (8,9). In both cases, off-target binding resulted in faster than expected elimination in a particular species. When off-target clearance is suspected in preclinical species, preclinical PK data may offer less predictive value for human PK properties. Furthermore, fast clearance due to off-target binding may result in the need for significantly higher clinical doses to achieve the desired drug exposure. Off-target binding not only poses challenges to predicting human PK, but may also lead to potential safety risks. In some situations, it may be difficult to differentiate safety issues associated with specific-target binding and off-target binding, which may result in premature termination of a program pursuing a potentially valuable target. Therefore, careful evaluation of abnormal PK profiles observed in preclinical species can be used as a valuable component of clinical risk assessment and drug candidate selection in recombinant mAb therapeutic programs.

ACKNOWLEDGMENTS AND DISCLOSURES

The authors acknowledge the valuable technical advice from Drs Rong Deng and Saileta Prabhu from Genentech Inc. in reviewing the work. The authors thank *In Vivo* Studies Group at Genentech for conducting the mouse and rat PK study, Derek Kennedy for coordinating the monkey studies, and Rashell Kinard for bioanalytic contributions. We would like to extend our thanks to Drs Christina de Zafra, Rodney Prell, Gary Cain, Ryan Watts, and Y. Gloria Meng for their contribution to the program.

Authors are employees at Genentech/Roche and hold Roche stocks.

REFERENCES

1. Dirksand NL, Meibohm B. Population pharmacokinetics of therapeutic monoclonal antibodies. Clin Pharmacokinet. 2010;49:633–59.
2. Lobo ED, Hansen RJ, Balthasar JP. Antibody pharmacokinetics and pharmacodynamics. J Pharm Sci. 2004;93:2645–68.
3. Mager DE. Target-mediated drug disposition and dynamics. Biochem Pharmacol. 2006;72:1–10.
4. Roskos LK, Davis CG, Schwab GM. The clinical pharmacology of therapeutic monoclonal antibodies. Drug Dev Res. 2004;61:108–20.
5. Tabrizi MA, Tseng CM, Roskos LK. Elimination mechanisms of therapeutic monoclonal antibodies. Drug Discov Today. 2006;11:81–8.
6. Deng R, Iyer S, Theil FP, Mortensen DL, Fielder PJ, Prabhu S. Projecting human pharmacokinetics of therapeutic antibodies from nonclinical data: What have we learned? MAbs. 2010;3:61–6.
7. Ling J, Zhou H, Jiao Q, Davis HM. Interspecies scaling of therapeutic monoclonal antibodies: initial look. J Clin Pharmacol. 2009;49:1382–402.
8. Vugmeyster Y, Szklut P, Wensel D, Ross J, Xu X, Awwad M, Gill D, Tchistiakov L, Warner G. Complex pharmacokinetics of a humanized antibody against human amyloid Beta Peptide, anti-abeta ab2, in nonclinical species. Pharm Res. 2011;28:1696–706.
9. Bumbaca D, Wong A, Drake E, Reyes AE, 2nd, Lin BC, Stephan JP, Desnoyers L, Shen BQ, Dennis MS. Highly specific off-target binding identified and eliminated during the humanization of an antibody against FGF receptor 4. MAbs 2011;3:376–86..
10. Vugmeyster Y, Guay H, Szklut P, Qian MD, Jin M, Widom A, Spaulding V, Bennett F, Lowe L, Andreyeva T, Lowe D, Lane S,

Thom G, Valge-Archer V, Gill D, Young D, Bloom L. *In vitro* potency, pharmacokinetic profiles, and pharmacological activity of optimized anti-IL-21R antibodies in a mouse model of lupus. MAbs. 2010;2:335–46.
11. Bielenberg DR, Pettaway CA, Takashima S, Klagsbrun M. Neuropilins in neoplasms: expression, regulation, and function. Exp Cell Res. 2006;312:584–93.
12. Heand Z, Tessier-Lavigne M. Neuropilin is a receptor for the axonal chemorepellent Semaphorin III. Cell. 1997;90:739–51.
13. Kawasaki T, Kitsukawa T, Bekku Y, Matsuda Y, Sanbo M, Yagi T, Fujisawa H. A requirement for neuropilin-1 in embryonic vessel formation. Development. 1999;126:4895–902.
14. Soker S, Takashima S, Miao HQ, Neufeld G, Klagsbrun M. Neuropilin-1 is expressed by endothelial and tumor cells as an isoform-specific receptor for vascular endothelial growth factor. Cell. 1998;92:735–45.
15. Bernatchez PN, Rollin S, Soker S, Sirois MG. Relative effects of VEGF-A and VEGF-C on endothelial cell proliferation, migration and PAF synthesis: Role of neuropilin-1. J Cell Biochem. 2002;85:629–39.
16. Chen H, He Z, Bagri A, Tessier-Lavigne M. Semaphorin-neuropilin interactions underlying sympathetic axon responses to class III semaphorins. Neuron. 1998;21:1283–90.
17. Fujisawa H. From the discovery of neuropilin to the determination of its adhesion sites. Adv Exp Med Biol. 2002;515:1–12.
18. Mamluk R, Gechtman Z, Kutcher ME, Gasiunas N, Gallagher J, Klagsbrun M. Neuropilin-1 binds vascular endothelial growth factor 165, placenta growth factor-2, and heparin via its b1b2 domain. J Biol Chem. 2002;277:24818–25.
19. Cackowski FC, Xu L, Hu B, Cheng SY. Identification of two novel alternatively spliced Neuropilin-1 isoforms. Genomics. 2004; 84:82–94.
20. Rossignol M, Gagnon ML, Klagsbrun M. Genomic organization of human neuropilin-1 and neuropilin-2 genes: identification and distribution of splice variants and soluble isoforms. Genomics. 2000;70:211–22.
21. Gagnon ML, Bielenberg DR, Gechtman Z, Miao HQ, Takashima S, Soker S, Klagsbrun M. Identification of a natural soluble neuropilin-1 that binds vascular endothelial growth factor: *In vivo* expression and antitumor activity. Proc Natl Acad Sci U S A. 2000;97:2573–8.
22. Lu Y, Xiang H, Liu P, Tong RR, Watts RJ, Koch AW, Sandoval WN, Damico LA, Wong WL, Meng YG. Identification of circulating neuropilin-1 and dose-dependent elevation following anti-neuropilin-1 antibody administration. MAbs. 2009;1:364–9.
23. Pan Q, Chathery Y, Wu Y, Rathore N, Tong RK, Peale F, Bagri A, Tessier-Lavigne M, Koch AW, Watts RJ. Neuropilin-1 binds to VEGF121 and regulates endothelial cell migration and sprouting. J Biol Chem. 2007;282:24049–56.
24. Liang WC, Dennis MS, Stawicki S, Chanthery Y, Pan Q, Chen Y, Eigenbrot C, Yin J, Koch AW, Wu X, Ferrara N, Bagri A, Tessier-Lavigne M, Watts RJ, Wu Y. Function blocking antibodies to neuropilin-1 generated from a designed human synthetic antibody phage library. J Mol Biol. 2007;366:815–29.
25. Pan Q, Chanthery Y, Liang WC, Stawicki S, Mak J, Rathore N, Tong RK, Kowalski J, Yee SF, Pacheco G, Ross S, Cheng Z, Le Couter J, Plowman G, Peale F, Koch AW, Wu Y, Bagri A, Tessier-Lavigne M, Watts RJ. Blocking neuropilin-1 function has an additive effect with anti-VEGF to inhibit tumor growth. Cancer Cell. 2007;11:53–67.
26. Xin Y, Xiang H, Dresser M, Brachmann RK, Bai S. Characterization of MNRP1685A (anti-NRP1) Clinical Pharmacokinetics in a first-in-human Phase I Study. AAPS National Biotechnology Conference (2010).
27. Gibiansky L, Gibiansky E, Kakkar T, Ma P. Approximations of the target-mediated drug disposition model and identifiability of model parameters. J Pharmacokinet Pharmacodyn. 2008;35:573–91.
28. Dedrick RL. Animal scale-up. J Pharmacokinet Biopharm. 1973;1:435–61.
29. Lu JF, Bruno R, Eppler S, Novotny W, Lum B, Gaudreault J. Clinical pharmacokinetics of bevacizumab in patients with solid tumors. Cancer Chemother Pharmacol. 2008;62:779–86.
30. Bruno R, Washington CB, Lu JF, Lieberman G, Banken L, Klein P. Population pharmacokinetics of trastuzumab in patients with HER2+ metastatic breast cancer. Cancer Chemother Pharmacol. 2005;56:361–9.
31. Ng CM, Lum BL, Gimenez V, Kelsey S, Allison D. Rationale for fixed dosing of pertuzumab in cancer patients based on population pharmacokinetic analysis. Pharm Res. 2006;23:1275–84.
32. Bumbaca D, Xiang H, Boswell CA, Port RE, Stainton SL, Mundo EE, Ulufatu S, Bagri A, Theil FP, Fielder PJ, Khawli LA, Shen BQ. Maximizing tumor exposure to anti-neuropilin-1 antibody requires saturation of non-tumor tissue antigenic sinks in mice. Br J Pharmacol. 2012;166:368–77.
33. Ma P, Yang BB, Wang YM, Peterson M, Narayanan A, Sutjandra L, Rodriguez R, Chow A. Population pharmacokinetic analysis of panitumumab in patients with advanced solid tumors. J Clin Pharmacol. 2009;49:1142–56.
34. Kloft C, Graefe EU, Tanswell P, Scott AM, Hofheinz R, Amelsberg A, Karlsson MO. Population pharmacokinetics of sibrotuzumab, a novel therapeutic monoclonal antibody, in cancer patients. Invest New Drugs. 2004;22:39–52.
35. Hansel DE, Wilentz RE, Yeo CJ, Schulick RD, Montgomery E, Maitra A. Expression of neuropilin-1 in high-grade dysplasia, invasive cancer, and metastases of the human gastrointestinal tract. Am J Surg Pathol. 2004;28:347–56.
36. Darbonne WC, Du X, Dhawan P, Hartley D, Tarrant J, Taylor H, Cain G, Shih LM, Brachmann RK, Phung Q, Weekes CD, LoRusso P, Patnaik A, Xiang H, Ramakrishnan V. Mechanism for platelet reduction in anti-neuropilin-1 (MNRP1685A)–treated phase I patients. J Clin Oncol. 2011, 29: suppl; abstr e13598.